

Experimental scaling of the scrape-off layer particle flux width by outboard divertor Langmuir probes with favorable B_t configuration on EAST

X. Liu¹, L. Y. Meng¹, J. C. Xu², L. Wang^{1,3,*}, J. Li^{1,3}, and the EAST Team

¹*Institute of Plasma Physics, Chinese Academy of Sciences, Hefei 230031, People's Republic of China*

²*School of Mechanical Engineering, Anhui University of Science & Technology, Huainan 232001, People's Republic of China*

³*Institute of Energy, Hefei Comprehensive National Science Centre, Hefei 230031, People's Republic of China*

*E-mail: lwang@ipp.ac.cn

Abstract

The scrape-off layer (SOL) power width (λ_q) is important for predicting the heat load on divertor targets for future magnetically confined devices. However, there're still some inconsistencies between the experimental and simulation results for λ_q scaling. This paper extends the previous SOL particle flux width (λ_{js} , $\lambda_q \approx \lambda_{js}$ is assumed for EAST divertor probe measurements) scaling [Liu *et al* 2019 *Plasma Phys. Control. Fusion* 61 045001] and provides more experimental evidence to support the λ_q study. A systematic method has been developed to calibrate the upper outer (UO) divertor Langmuir probes (Div-LPs) with the Ohmic discharges to reduce the measurement uncertainty of λ_{js} . For the discharges with the favorable B_t and upper single null configurations in the 2019 EAST experiment campaign, about 260 discharges have been filtered out. The calibrated j_s data measured by the UO Div-LPs have been statistically analyzed. Three H-mode, L-mode, and Ohmic scaling databases have been constructed and are used for λ_{js} scalings. It is found that the outboard λ_{js} for H-mode and L-mode plasmas scales as, $\lambda_{js,UO} = 2.21(W_{MHD}/\bar{n}_e)^{-0.52}$, where W_{MHD} is the stored energy and \bar{n}_e is the line-averaged density. This scaling is consistent with the inboard λ_{js} scaling in the previous work. If stiff plasma profiles are assumed, the obtained λ_{js} scaling has a negative scaling dependence on the edge plasma temperature, which is in agreement with the simulation result [Liu *et al* 2019 *Phys. Plasmas* 26 042509] by the BOUT-HESEL code. This makes the λ_q prediction for the ITER 15 MA H-mode baseline scenario by this code more convincing [Liu *et al* 2022 *Nucl. Fusion* 62 076022].

Keywords: scrape-off layer particle flux width, divertor Langmuir probe, EAST

1. Introduction

It is well known that the divertor heat load is a crucial problem for future magnetically confined fusion devices due to the engineering limit of materials. The mitigation of the excessive

heat load on divertor targets needs a better understanding of the particle and heat transports in the edge and scrape-off layer (SOL). The SOL power width λ_q is an important parameter to characterize the heat transports in the SOL, which is determined by the competition between the radial and parallel heat transports. Currently, there are many experimental, theoretical, and numerical studies [1-15] have been carried out to scale λ_q and understand its underlying physics. As summarized in the introduction of reference [15], the physical mechanism of the SOL particle and heat transports is not fully understood. There still exist some inconsistencies between the experimental and numerical results, e.g., whether the radial heat transport in the SOL is dominated by the magnetic drift or turbulence, and if λ_q has a strong scaling dependence on the machine size. So, it is important to obtain more experimental results to validate the simulation results and confirm the hypothesis of the main physical mechanism responsible for the inconsistencies.

Previously, the divertor Langmuir probes (Div-LPs) have been used to measure the SOL particle flux width λ_{js} . The inboard λ_{js} scales as, $\lambda_{js,UI,H} = 0.85(W_{MHD}/\bar{n}_e)^{-0.50}P_{tot}^{-0.06}$, where W_{MHD} is the stored energy, \bar{n}_e is the line-averaged density, and P_{tot} is the total input power [7]. However, with the upper single null (USN) and forward (unfavorable) toroidal magnetic field (B_t) configurations and the low hybrid wave (LHW) heating scheme, the upper outer (UO) strike point normally splits [16]. This leads to the use of upper inner (UI) Div-LP data for λ_{js} scaling in the previous work. Since the outboard λ_{js}/λ_q is normally used for scaling, whether the outboard λ_{js} follows the same scaling dependence on W_{MHD}/\bar{n}_e requires further investigation, which is the main motivation for this paper.

For a certain probe tip, the measured particle flux is $\Gamma = j_s/e$, where e is the elementary charge, and j_s is the ion saturated current density. j_s is normally calculated with $j_s \equiv C_h I_s / A_h$, where I_s is the ion saturated current, A_h is the designed collecting area of the tip head, and C_h is the calibration coefficient. Since the actual collecting area is hard to evaluate and is changing during the experimental campaign by the erosion process [17], C_h is introduced. Then the actual collection area of the probe tip is A_h/C_h . At the start of one experiment campaign, C_h is typically set to be unity. During the experiment campaign, C_h is normally adjusted manually by experience. To minimize the uncertainty of the measurement of j_s and further the fitting for λ_{js} , a systematic calibration method has been introduced to calibrate C_h in this paper before scaling λ_{js} . The rest of this paper is organized as follows: Section 2 introduces the basic experimental conditions for the selected discharges; section 3 describes the method and procedure of the calibration of the UO Div-LPs; section 4 constructs the scaling databases, scales λ_{js} , and compares and discusses the obtained λ_{js} scaling with previous studies; section 5 summarizes the whole paper.

2. Experiment conditions

The basic machine parameters of EAST [18], the divertor shape and materials (ITER-like tungsten/copper divertors [19] for upper divertors), and the employed main diagnostics (Div-LPs [20]) are described in section 2.1 of reference [7]. The employed Div-LPs located at the upper divertors have two toroidally asymmetric arrays. The first and second Div-LP arrays locate at the D and O ports (toroidal displacement is 112.5°), respectively. Since we aim to scale the outboard

λ_{js} with the UO Div-LPs, the discharges that are configured with USN geometry, and reversed (or favorable) toroidal magnetic field (the ion $\mathbf{B} \times \nabla B$ drift velocity directs upwards) are typically selected to avoid strike point splitting. The selected discharges in the 2019 experiment campaign range from #86377 to #88018. Note that from #86790 to #87475, most of the discharges are helium (or mixed with deuterium) plasmas. To ensure the reliability of the Div-LP calibration in the next section, these discharges are included in the calibration procedure. In this paper, we focus on the scaling of λ_{js} in deuterium plasmas, and the scaling of λ_{js} in helium plasmas will be performed in future work. The discharges are classified into three types: the Ohmic discharges, the L-mode discharges, and the H-mode discharges. For the Type-I ELMy H-mode discharges, only the inter-ELM Div-LP data are retained. For the ELM-free or Grassy ELMy H-mode discharges, the data processing procedure is kept the same as that for the L-mode discharges. The heating scheme typically utilized radio-frequency waves (LHW and/or electron cyclotron resonance heating). The plasma was fueled with supersonic molecular beam injection and the wall was coated with lithium. The discharges with divertor impurity seeding or resonant magnetic perturbation are omitted in the scaling databases. The main plasma and engineering parameters in the scaling databases are shown in figure 5.

3. Calibration of the divertor Langmuir probes

As mentioned in the introduction, the sparse poloidal distribution, the independent measurement characteristic, and the relatively large measurement uncertainties of the Div-LPs challenge the accurate evaluation of λ_{js} . Benefiting from the two toroidally distributed Div-LP arrays (UO-D and UO-O, see figure 1 in reference [7]) embedded in the UO divertors, it is possible to calibrate the measurement coefficients of j_s by the Ohmic discharges to improve the evaluation accuracy of λ_{js} . An Ohmic discharge, #86568, is selected as the starting calibration point. Figure 1 shows the j_s profile (averaged in 50 ms) mapped to the outboard midplane (OMP) for the UO-D and UO-O Div-LP measurements. The red solid line represents the Eich fit (see equation 2 in reference [7]) based on the UO-O Div-LP measurements. The fitted λ_{js} is close to $\lambda_{js,EAST}$ calculated by the EAST L-mode λ_q scaling [4], demonstrating the reliability of the UO-O Div-LP calibration coefficients. The numbers in figure 1 mark the channel number of the UO-D and UO-O Div-LPs. Since normally the j_s profile at the divertor target can be well fitted by the Eich function for the Ohmic discharges, calibration of the slightly biased Div-LPs is possible. For the Div-LP channels (e.g., channels 6~7) that deviate from the Eich fit, their calibration coefficients are modified to match the Eich fit. The calibrated coefficients by #86568 are then used as the starting calibration coefficients to calculate j_s .

To assist the calibration, the reliability of the UO Div-LPs needs to be evaluated. For all valid discharges, Div-LP j_s data are loaded with a time interval of one second in one discharge. Figure 2 plots the loaded j_s data normalized to the first data point ($j_{s,norm}$) for the main channels. The channels that have the same radial measurement positions for the UO-D and UO-O Div-LPs (the twin channels) are supposed to have similar $j_{s,norm}$. If there is a mismatch between them for a long

period, one of the channels shall be calibrated. The red vertical dashed lines represent the calibration points according to the final calibration results listed in table 2. The measurement reliabilities of one Div-LP can be evaluated by calculating the Pearson correlation coefficients (Corr) of $j_{s,norm}$ with its twin and adjacent channels. The results are shown in table 1, where the values of Corr that are larger than 0.7 are marked in bold. If the value of Corr between one channel and its twin or adjacent channel is marked in bold, the measurement reliability of this channel is treated as reliable. In the next step of the calibration, we refer to the reliable channels and the Eich fit to calibrate the not reliable channels with the Ohmic discharges.

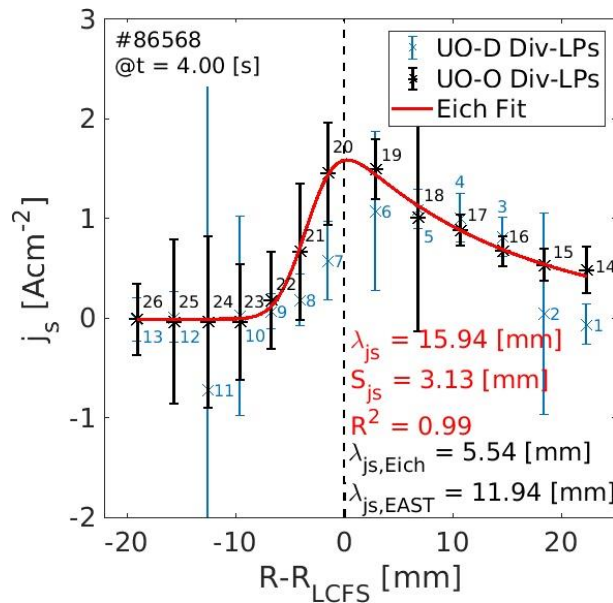


Figure 1 The calibration of Div-LPs with an Ohmic discharge as the starting calibration point. The red solid line represents the Eich fit of the UO-O Div-LP data. The dashed vertical line represents the separatrix. The numbers mark the channel number of the UO-D and UO-O Div-LPs. $\lambda_{js,Eich}$ and $\lambda_{js,EAST}$ are calculated by the Eich [2] and EAST L-mode [4] λ_q scalings, respectively.

The calibration procedure needs to check the fitting of the UO Div-LPs with the already calibrated coefficients for the remain uncalibrated Ohmic discharges. If the measurement of one channel is systematically larger or smaller than the Eich fit or the measurement by its twin channel for a series of Ohmic discharges, its calibration coefficient has to be adjusted. Figure 3 shows an example of calibrating the UO-O Div-LPs. The j_s profile for each Ohmic discharge is averaged around $t = 4$ s with a time interval of 50 ms. Discharge #86568 has been calibrated in the first step. From #86736 to #86868, j_s measured by channel 18 are always larger than those by its twin channel (channel 5). According to figure 2(c), the mismatch between channel 5 and channel 18 after #86568 firstly occurs at # 86685. Then we can calibrate the coefficient of channel 18 with #86736 and apply this coefficient starting from #86685. As the calibration goes, the information in figure 2 and table 1 is updated accordingly (the range of the uncalibrated discharges changes), helping to find out which channel should be calibrated. Note that, the calibration aims to calibrate the

systematically biased channels. If one channel is biased for a short period and restores afterward or oscillates around the Eich fit, this channel may reflect the real measurement and shall not be calibrated.

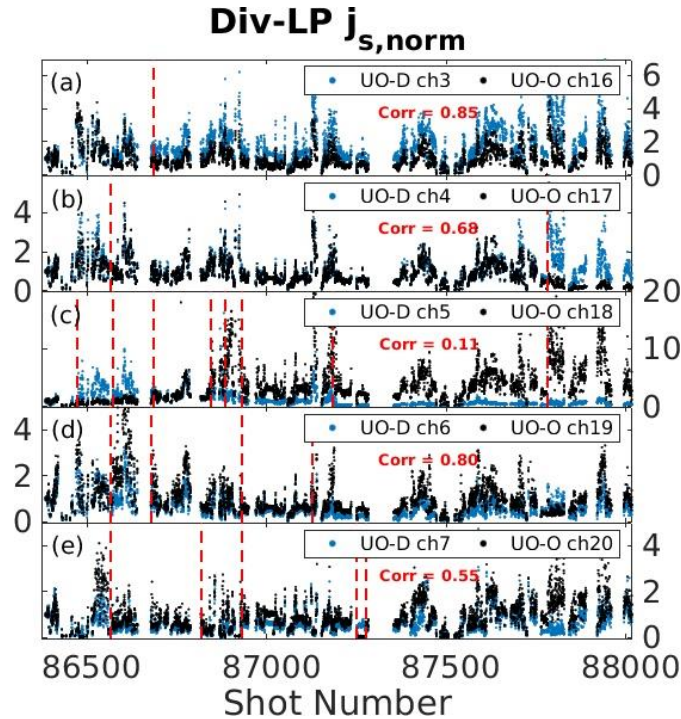


Figure 2 The evolution of Div-LP j_s data normalized to the first data point. The red dashed vertical lines represent the final calibration points for the corresponding UO-D and/or UO-O Div-LP channels.

Table 1. The Pearson correlation coefficients (Corr) of $j_{s,norm}$ for the UO Div-LPs.

Corr	UO-D Ch. N	UO-D Ch. N	UO-D Ch. N	UO-O Ch. N	UO-O Ch. N
	UO-O Ch. N	UO-O Ch. $N+1$	UO-D Ch. $N+1$	UO-O Ch. $N+1$	UO-D Ch. $N+1$
Channel 1/14	0.3828	0.3810	0.4017	0.9539	0.5772
Channel 2/15	0.6057	0.5604	0.8320	0.9498	0.8604
Channel 3/16	0.8475	0.5672	0.8801	0.6804	0.8905
Channel 4/17	0.6849	0.6091	0.3657	0.3147	0.4601
Channel 5/18	0.1072	0.3640	0.3981	0.1185	0.0790
Channel 6/19	0.8033	0.1632	0.2828	0.0951	0.2468
Channel 7/20	0.5486	0.7242	0.6824	0.2344	0.2307
Channel 8/21	0.7471	0.7635	0.6170	0.7467	0.4708
Channel 9/22	0.6668	0.7693	0.6825	0.7629	0.7031
Channel 10/23	0.8225	0.2827	0.5539	0.2729	0.4797
Channel 11/24	0.3122	0.5981	0.5354	0.4075	0.3115
Channel 12/25	0.8714	0.6392	0.4977	0.6246	0.4638
Channel 13/26	0.4375				

Note: N is the channel number. $N = 1 - 13$, and $14 - 26$ for the UO-D and UO-O Div-LPs, respectively. The values of Corr that are larger than 0.7 are marked in bold. The channel number in the first column is marked in bold if its correlation coefficients with its twin and/or adjacent channels are marked in bold.

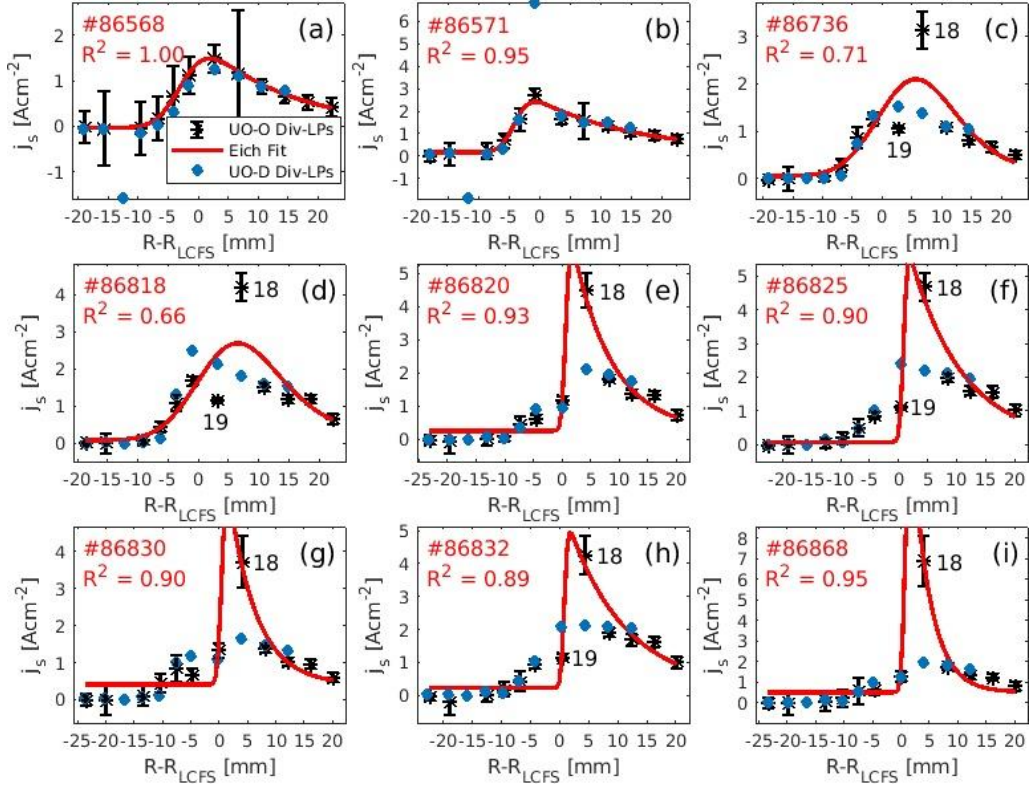


Figure 3 Calibration of the UO Div-LPs with Ohmic discharges. The red solid lines are Eich fit of the UO-O Div-LP data.

Table 2 lists the final calibration points for the UO Div-LPs. It seems that the UO-O Div-LPs are more reliable than the UO-D Div-LPs, as the number of channels that have been calibrated and the number of the calibration points for the calibrated channels are both smaller. This is further confirmed by the results shown in figure 4, where the coefficient of determination (R^2) is calculated for the j_s profile (the data around $t = 4$ s are selected for each discharge) fitted by the Eich function. The inserted picture shows the cumulative density function of R^2 . R^2 for the UO-O Div-LPs is more concentrated on the $R^2 = 1$. So, the UO-O Div-LPs are used for the evaluation of λ_{j_s} in this paper. Another reason for not using the UO-D Div-LP measurements is that the first two channels (lays inside the SOL, see figure 1) get malfunction for a long period, which greatly reduces the evaluation reliability of λ_{j_s} even though the fitting quality is good. Although the UO-D Div-LP measurements are not used, it helps to calibrate the twin channels of the UO-O Div-LPs, which indirectly influence the evaluation of λ_{j_s} in this paper.

Table 2. The final calibration points for the UO Div-LPs.

	UO-D Calibration Points	UO-O Calibration Points
Channel 1/14	86378 87782	
Channel 2/15	86378 86685	
Channel 3/16	86685	
Channel 4/17	86378 86568	87782
Channel 5/18	86378 86475 86685 86845 86931 87183	86572 86685 86844 86884 86931 87782
Channel 6/19	86378 86568 86678 87127	86678 86931
Channel 7/20	86568 86818 86931	86931 87250 87276
Channel 8/21	86568 86931 87724	
Channel 9/22	86868 87615 87782	
Channel 10/23	86868	
Channel 11/24	86569 86678 86868	86378
Channel 12/25	86868	
Channel 13/26	86868	

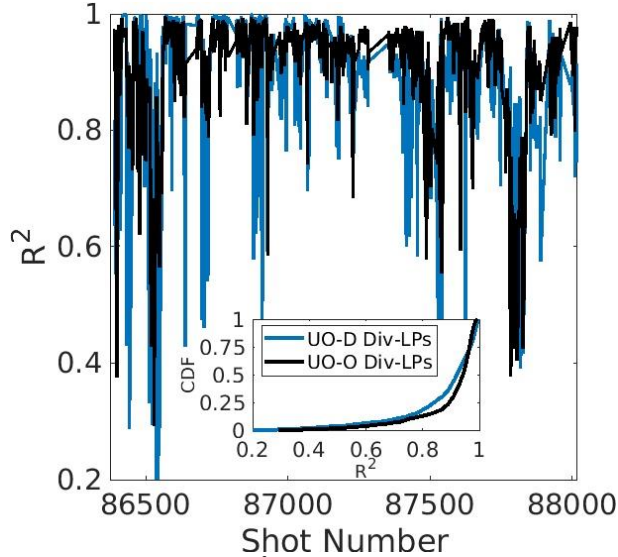


Figure 4 The coefficient of determination (R^2) of the j_s profile fitting for the UO-D and UO-O Div-LPs. The inserted picture shows the corresponding cumulative density function (CDF) of R^2 .

4. Scalings of the SOL particle flux width

In this section, we use the calibrated UO-O Div-LP j_s coefficients to calculate λ_{js} for the deuterium plasmas in favorable B_t configuration. Almost all the discharges from #86790 to #87475 are omitted, leaving about 900 discharges for statistical analysis. The filter techniques and the scaling procedures used in this paper are described detailedly in reference [7]. The UO-O Div-LP j_s data are pre-fitted (only 20 profiles are selected and fitted) for each of the ~ 900 discharges. With the pre-fitted results, a filter of the discharges is carried out by the following selection criteria: $R^2 \geq 0.88$, the number of main measurement points $n_{main} \geq 4$, the ratio of the minimum value of the

SOL measurements to the maximum value of the whole measurements $r_{SOL-min,peak} < 0.45$, and the ratio of the outermost SOL measurement (by channel 14) to the minimum value of the whole measurements $r_{SOL,tail} < 0.15$ for each fit of the j_s profile in one discharge, and the number of good fit $n_{good} \geq 10$ for each discharge. The time ranges of the confinement types of the 269 discharges that passed the filter process are marked and classified into the H-mode, L-mode, and Ohmic types. For each confinement type, the j_s data are refitted with an averaging time interval of 50 ms and selected again manually by checking the fitting results. Finally, 129 H-mode discharges, 103 L-mode discharges, and 32 Ohmic discharges are used for constructing the scaling databases.

Three (H-mode, L-mode, and Ohmic) scaling databases are constructed by collecting λ_{js} , the spreading factor of parallel particle flux S_{js} , R^2 , B_t , the poloidal magnetic field at the last closed flux surface (LCFS) on the OMP B_p , the plasma current I_p , the safety factor at the 95% flux surface q_{95} , W_{MHD} , \bar{n}_e , P_{tot} , the plasma elongation κ , the triangularity δ , etc. The distribution of the main plasma and engineering parameters is shown in figure 5. The distributions of λ_{js} peak around $\lambda_{js} = 10.5$ mm for both H-mode and L-mode scaling databases. The standard deviations (2% of the data in the head and tail of the distribution are removed in the calculation) for B_t , B_p , and q_{95} are smaller than those for \bar{n}_e , W_{MHD} , and P_{tot} . The values of the peaks of \bar{n}_e , W_{MHD} , and P_{tot} distributions increase for the Ohmic, L-mode, and H-mode scaling databases, meeting our expectations.

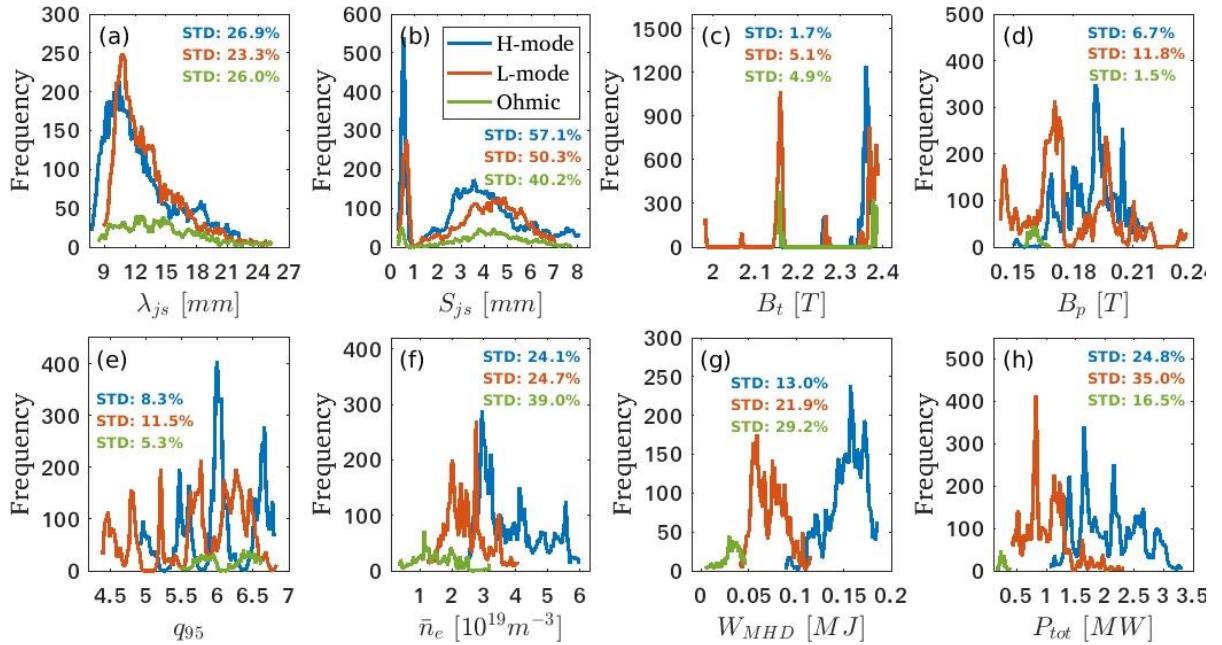


Figure 5 The distributions of the main plasma and engineering parameters for the scaling databases. The standard deviation (STD) is calculated by removing 2% of the data in the head and tail of the distribution.

According to the previous study in reference [7] and the results shown in figure 5, we start the non-linear multi-variable regressions ($\lambda_{js} = C_0 \prod_{i=1}^n x_i^{C_i}$, where x_i is the scaling parameter, C_i is the scaling coefficients, and i is the non-zero natural number) with the parameters that have large

variances. For the H-mode scaling database, the regression result is listed as #1H in table 3. Since λ_{js} has almost no correlation with q_{95} (see table 4), q_{95} is omitted for #2H. To further minimize the scaling parameter, P_{tot} can also be omitted due to its relatively large correlation with \bar{n}_e . From the regression result of #3H, λ_{js} has a strong positive scaling dependence on \bar{n}_e , and a negative scaling dependence on W_{MHD} . This is quite similar to the inboard λ_{js} scaling (#4 in table 4 of reference [7]). Similarly, we combine W_{MHD} and \bar{n}_e as one scaling parameter and the result is listed as #4H. #5H ($\lambda_{js,UO,H} = 1.55(W_{MHD}/\bar{n}_e)^{-0.56}P_{tot}^{0.41}$) is obtained for comparison with the inboard λ_{js} scaling ($\lambda_{js,UI,H} = 0.85(W_{MHD}/\bar{n}_e)^{-0.50}P_{tot}^{-0.06}$) in reference [7]. Obviously, the outboard λ_{js} scaling has stronger scaling dependences on the scaling parameters and a nearly twice scaling amplitude. For the L-mode scaling database, a similar procedure has been carried out and the results are listed from #1L to #4L in table 3. Note that the λ_{js} scalings for the H-mode (#4H) and L-mode (#4L) databases are quite similar, and the scaling parameter ranges are different for the H-mode and L-mode plasmas (see figure 5). We combine the H-mode and L-mode scaling databases, and obtain the scaling #1HL,

$$\lambda_{js,UO} = (2.21 \pm 0.07)(W_{MHD}/\bar{n}_e)^{-0.52 \pm 0.01}. \quad (1)$$

Compared with #4H and #4L, #1HL has a slightly smaller R^2 and a weaker scaling exponent, but a more consistent scaling exponent with the inboard λ_{js} scaling. The detailed scaling results for #4H, #4L, and #1HL are shown in figure 6.

Table 3. The non-linear regression results of λ_{js} for the H-mode and L-mode scaling databases.

#	C_0	$C_{q_{95}}$	$C_{\bar{n}_e}$	$C_{W_{MHD}}$	C_{W_{MHD}/\bar{n}_e}	$C_{P_{tot}}$	R^2
1H	0.62 (0.05)	0.67 (0.05)	0.74 (0.02)	-0.31 (0.03)		0.34 (0.01)	0.66
2H	1.55 (0.07)		0.67 (0.02)	-0.51 (0.02)		0.31 (0.01)	0.62
3H	1.70 (0.08)		0.82 (0.02)	-0.47 (0.02)			0.51
4H	1.70 (0.08)				-0.62 (0.01)		0.48
5H	1.55 (0.07)				-0.56 (0.01)	0.41 (0.01)	0.62
1L	0.66 (0.03)	0.63 (0.03)	0.38 (0.01)	-0.58 (0.02)		0.25 (0.01)	0.61
2L	1.35 (0.08)	0.43 (0.03)	0.47 (0.01)	-0.41 (0.02)			0.54
3L	2.10 (0.10)		0.48 (0.01)	-0.52 (0.02)			0.51
4L	1.58 (0.08)				-0.60 (0.01)		0.54
1HL	2.21 (0.07)				-0.52 (0.01)		0.45

Note: The values in the parenthesis are the errors of the regression coefficients. The H-mode and L-mode regressions are marked with H and L as the suffix of the regression number (#).

According to the results in references [3,4,7], λ_{js} is approximately equal to λ_q for the Div-LP measurements. Then we can compare the measured λ_{js} in the databases with the λ_q scalings in

previous studies. Figure 7 scales λ_{js} against B_p and compares this scaling with the Eich [2] and EAST H-mode [3] λ_q scalings. Although the obtained λ_{js} scaling (black solid line) has a relatively poor regression quality ($R^2 = 0.18$), its scaling dependence on B_p is almost the same as that for the Eich (red solid line) and EAST (purple solid line) H-mode scalings. However, the scaling amplitude of the λ_{js} scaling is ~ 3 and ~ 1.6 times larger than that for the Eich and EAST λ_q scalings, respectively. Even though the previous explanation for this different scaling amplitude relies on the radio-frequency heating scheme in EAST, the data from the Ohmic database do not follow the Eich scaling in figure 7, indicating that there exist some unknown physical mechanisms that broaden λ_{js}/λ_q in EAST. Different from the λ_q scalings [5] in AUG, the H-mode λ_{js} scaling is similar to the L-mode λ_{js} scaling in the scaling amplitude. This might result from that the edge plasma parameters for the H-mode and L-mode plasmas in EAST are similar. Still, the characteristic that the H-mode and L-mode λ_{js} scalings can be unified (equation 1) is the same as that for the C-Mod ($\lambda_{q,C-Mod} = 0.91\bar{p}^{-0.48}$, where \bar{p} is the volume-averaged core plasma pressure) [6] and AUG ($\lambda_{q,AUG} = 7.57\bar{p}^{-0.52}$) [8] λ_q scalings, where the H-mode, I-mode, and L-mode data converge to a single scaling. Furthermore, the scaling exponent of \bar{p} is also nearly the same as that for the scaling exponent of W_{MHD} in the λ_{js} scaling (W_{MHD} is positively correlated with \bar{p}). So, the pure scaling dependence of λ_{js}/λ_q on B_p cannot cover the whole physics. The scaling dependences on some main plasma parameters (W_{MHD} , \bar{p} , and/or \bar{n}_e) are required to better respond to the physics of SOL heat transport, even though generally B_p is correlated with these main plasma parameters. When the λ_{js}/λ_q scaling has a wide variance of B_p (like the Eich scaling, where the multi-machine database is employed), the correlation between B_p and the main plasma parameters is significant. While for one specific machine with a relatively narrow operating regime, the variance of B_p is smaller compared with the main plasma parameters (see figure 5), resulting in a weaker correlation between λ_{js} and B_p (see figure 7). This point of view agrees with the results in reference [9], where the scaling dependence of λ_q on B_p is modified by a turbulence-driven broadening mechanism.

Table 4. The Pearson correlation coefficients (Corr) of the scaling parameters for the H-mode and L-mode scaling databases.

H-mode (L-mode) Corr	q_{95}	\bar{n}_e	W_{MHD}	P_{tot}
λ_{js}	0.05 (0.36)	0.68 (0.51)	-0.29 (-0.46)	0.56 (0.02)
q_{95}		-0.34 (-0.01)	-0.51 (-0.40)	-0.13 (-0.16)
\bar{n}_e			-0.02 (0.05)	0.44 (0.31)
W_{MHD}				-0.07 (0.61)

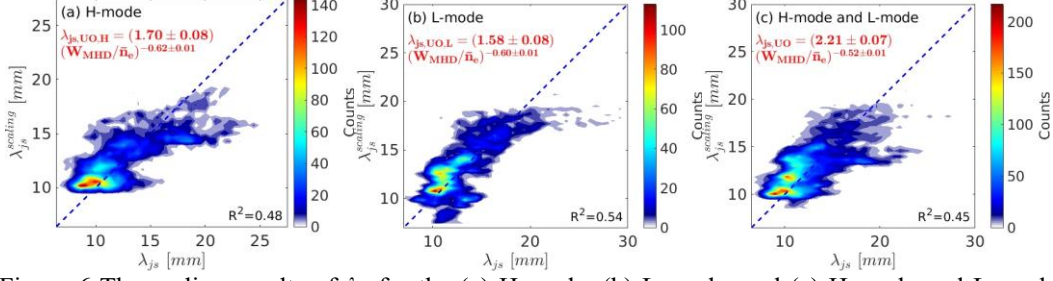


Figure 6 The scaling results of λ_{js} for the (a) H-mode, (b) L-mode, and (c) H-mode and L-mode combined databases.

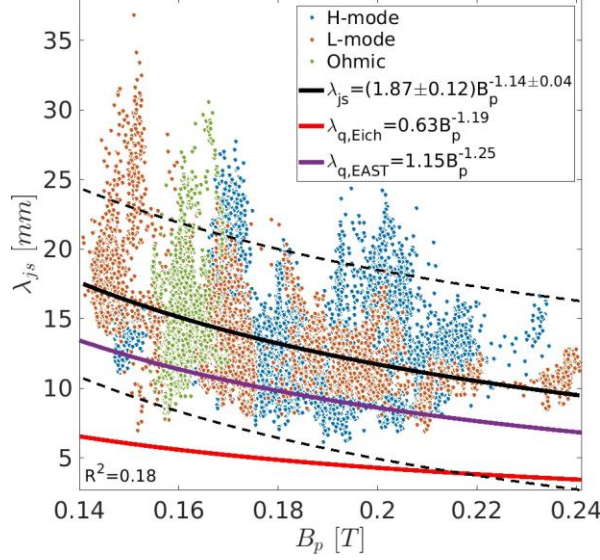


Figure 7 The scaling of λ_{js} against B_p with all three databases and the comparisons with the Eich [2] and EAST H-mode [3] λ_q scalings. The black dashed lines represent the scaling uncertainties.

As discussed in references [5,7], if we assume stiff plasma profiles, $W_{MHD}/\bar{n}_e \propto T_{e,LCFS}$, where $T_{e,LCFS}$ is the electron temperature at the LCFS on the OMP. Then the UO λ_{js} scaling in equation 1 becomes, $\lambda_{js,UO} \propto T_{e,LCFS}^{-0.52}$. The negative scaling dependence on the edge plasma temperature is consistent with the simulation results by the BOUT-HESEL code [14,15] and is against the theoretical λ_n scaling by the heuristic drift-based model [11]. The BOUT-HESEL simulation results claim that the radial heat transport in the SOL for EAST H-mode and L-mode plasmas is dominated by the electrostatic turbulences rather than the magnetic drift [15]. Then the physical mechanism of the negative scaling dependence of UO λ_{js} on the edge plasma temperature is that the increase of the edge plasma temperature enhances the parallel particle/heat transport (mainly through the electron conduction) and weakens the radial turbulent particle/heat transport, resulting in a narrower parallel particle/heat profile in the radial direction, and hence a smaller λ_{js}/λ_q . The λ_{js} scaling in this paper validates the simulation results by the BOUT-HESEL code and the hypothesis that explains the inconsistencies between the experimental and the simulation results (see section 5 of reference [15]), which makes the simulated λ_q for the ITER 15 MA baseline scenario more convincible.

5. Summaries

In this paper, a systematic method has been developed to calibrate the Div-LPs, which normally have large measurement uncertainties for λ_{js} . The calibration procedure relies on the two toroidally asymmetric Div-LP arrays and the Ohmic discharges. By examining the Pearson correlation coefficients between one channel and its twin and adjacent channels, the measurement uncertainty of this channel can be roughly evaluated. The calibration has been performed for the channels that have large measurement uncertainties by checking their performance for a long period with the selected Ohmic discharges. According to the calibration results, the UO-O Div-LP array performs better than the UO-D Div-LP array, and it is chosen for the scaling of outboard λ_{js} in favorable B_r configuration.

About 900 deuterium discharges have been filtered by evaluating the fitting quality of the measured j_s profile, leaving 129 H-mode discharges, 103 L-mode discharges, and 32 Ohmic discharges for constructing the scaling databases. The non-linear regressions of λ_{js} have been carried out with respect to the parameters that have large variances for the H-mode and L-mode databases. It is found that the outboard λ_{js} has a negative scaling dependence on W_{MHD}/\bar{n}_e , e.g., $\lambda_{js,UO} = 2.21(W_{MHD}/\bar{n}_e)^{-0.52}$, similar to that in the previous work [7] for the inboard λ_{js} scaling ($\lambda_{js,UI,H} = 0.85(W_{MHD}/\bar{n}_e)^{-0.50}P_{tot}^{-0.06}$). This scaling can be explained by the BOUT-HESEL simulations [14,15] and validates the simulation code experimentally. Furthermore, the scaling fits for both the H-mode and L-mode scaling databases and has better regression quality compared with the scaling using B_p as the scaling parameter, indicating that solely scaling of λ_{js}/λ_q with respect to the engineering parameters is not enough and the main plasma parameter shall be included.

Acknowledgments

This work was supported by the Natural Science Foundation of China (Nos. 12005260, 11922513), and the National Key Research and Development Program (Nos. 2017YFE0301300, 2018YFE0303104). This work was also partially supported by the Institute of Energy, Hefei Comprehensive National Science Center under Grant No. GXXT-2020-004.

References

- 1 Eich T *et al* 2011 *Phys. Rev. Lett.* 107 215001
- 2 Eich T *et al* 2013 *Nucl. Fusion* 53 093031
- 3 Wang L *et al* 2014 *Nucl. Fusion* 54 114002
- 4 Liu J B *et al* 2015 *Fusion Eng. Des.* 100 301–6

- 5 Sieglin B *et al* 2016 *Plasma Phys. Controlled Fusion* 58 055015
- 6 Brunner D *et al* 2018 *Nucl. Fusion* 58 094002
- 7 Liu X *et al* 2019 *Plasma Phys. Control. Fusion* 61 045001
- 8 Silvagni D *et al* 2020 *Plasma Phys. Control. Fusion* 62 045015
- 9 Eich T *et al* 2020 *Nucl. Fusion* 60 056016
- 10 Horacek J *et al* 2020 *Nucl. Fusion* 60 066016
- 11 Goldston R J *et al* 2012 *Nucl. Fusion* 52 013009
- 12 Chang C S *et al* 2017 *Nucl. Fusion* 57 116023
- 13 Xu X Q *et al* 2019 *Nucl. Fusion* 59 126039
- 14 Liu X *et al* 2019 *Phys. Plasmas* 26 042509
- 15 Liu X *et al* 2022 *Nucl. Fusion* 62 076022
- 16 Feng W *et al* 2017 *Nucl. Fusion* 57 126054
- 17 Meng L Y *et al* 2021 *Nuclear Materials and Energy* 27 100996
- 18 Wan B N *et al* 2015 *Nucl. Fusion* 55 104015
- 19 Luo G-N *et al* 2017 *Nucl. Fusion* 57 065001
- 20 Xu J C *et al* 2016 *Rev. Sci. Instrum.* 87 083504
- 21 Wang L *et al* 2017 *Nuclear Materials and Energy* 12 221